Nanoscale Electrical Probes on a Single Facet of a ZnO Microwire
Device Fabrication and Local Electrical Characteristics

Yun, Yoojoo; Shin, Dong Hoon; Kim, Hakseong; Choi, Jun Hee; Jeong, Hyunjeong; Suh, Dongseok; Kang, Haeyong; Lee, Sang Wook

DOI
10.1021/acsaelm.2c00179

Publication date
2022

Document Version
Final published version

Published in
ACS Applied Electronic Materials

Citation (APA)
Yun, Y., Shin, D. H., Kim, H., Choi, J. H., Jeong, H., Suh, D., Kang, H., & Lee, S. W. (2022). Nanoscale Electrical Probes on a Single Facet of a ZnO Microwire: Device Fabrication and Local Electrical Characteristics. *ACS Applied Electronic Materials*, *4*(5), 2346-2352. https://doi.org/10.1021/acsaelm.2c00179

ACS APPLIED ELECTRONIC MATERIALS

pubs.acs.org/acsaelm Article

Nanoscale Electrical Probes on a Single Facet of a ZnO Microwire: Device Fabrication and Local Electrical Characteristics

Yoojoo Yun,[▽] Dong Hoon Shin,[▽] Hakseong Kim,[▽] Jun Hee Choi, Hyunjeong Jeong, Dongseok Suh, Haeyong Kang,* and Sang Wook Lee*

Cite This: *ACS Appl. Electron. Mater.* 2022, 4, 2346−2352 Read Online

ACCESS | Metrics & More | Article Recommendations | Supporting Information

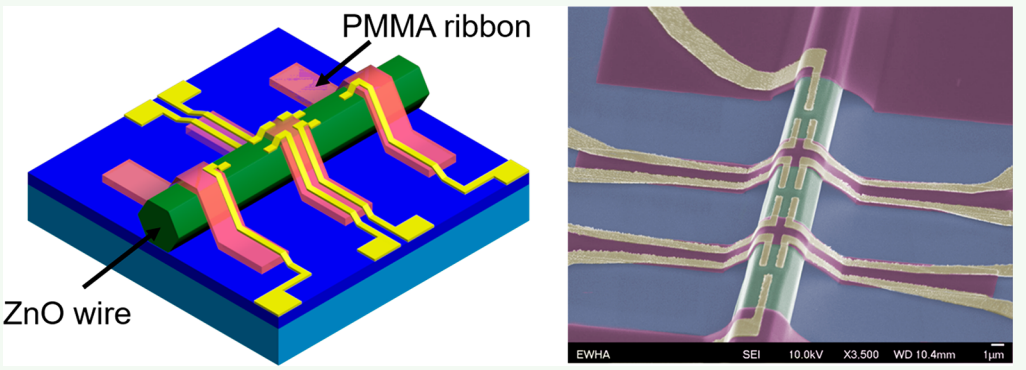

ABSTRACT: The electrical properties of a single facet of an individual ZnO microwire were investigated. Electrode patterns with a Hall bar structure were deposited on the surface of the top facet of the ZnO microwire. Using a suspended and cross-linked poly(methyl methacrylate) ribbon structure, it was possible to define the electrical connections only at the top surface, while avoiding those on the other five sides of the ZnO microwire. Current−voltage characteristics were examined, and Hall measurements were conducted with various magnetic fields. Through our device structure, the electrical properties could be directly probed at specific points on the ZnO surface in a reliable manner. The estimated electrical characteristics demonstrate that the carrier concentration and mobility of the ZnO surface varied along the axial direction of the wire. These results indicate that the charge carrier concentration on the surface of the micro-/nanowire can be sensitively changed according to the synthesis environment. In addition, it is worth noting that the nanoscale local Hall probes, fabricated by our technique, could probe the very slight variation of carrier concentration, which is difficult to detect by a standard transport measurement along the wire.

KEYWORDS: *ZnO microwire, PMMA cross-link, Hall measurement, carrier density, nanoscale local Hall probes, single-facet electrode structure*

1. INTRODUCTION

Zinc oxide (ZnO) with the crystal structure as shown in Figure 1a is one of the most widely studied semiconducting materials owing to its unique physical and chemical properties. Through coupling of its electrical, mechanical, and optical properties, ZnO exhibits multifunctional material and device characteristics.[1] ZnO nano-/microwire-based optoelectronic or electromechanical systems have gained special attention from scientists because of their superior device performance.[2,3] For example, light emission and lasing emission in the UV region with high directionality and high efficiency could be achieved from vertically aligned ZnO nanowire-based optoelectronic devices.[4−9] Piezoelectricity is another important property of the ZnO crystal structure. Efficient piezoelectric power generation has been reported for ZnO nano-/microwire-based electromechanical systems.[10−12] Although mature scientific knowledge has been attained during the past couple of decades, various emerging properties of ZnO nano-/microwire-based devices are being discovered via coupling of the electrical, mechanical, and optical degrees of freedom.

From the aforementioned developments in the ZnO research field, practical applications of ZnO-based nano-/microstructures, beyond scientific discovery, are being suggested and attempted. For this purpose, a consistent material property and reliable device performance are required as a first step. Several approaches have been reported for producing semiconductor nano-/microwire structures, includ-

Received: February 7, 2022
Accepted: May 1, 2022
Published: May 13, 2022

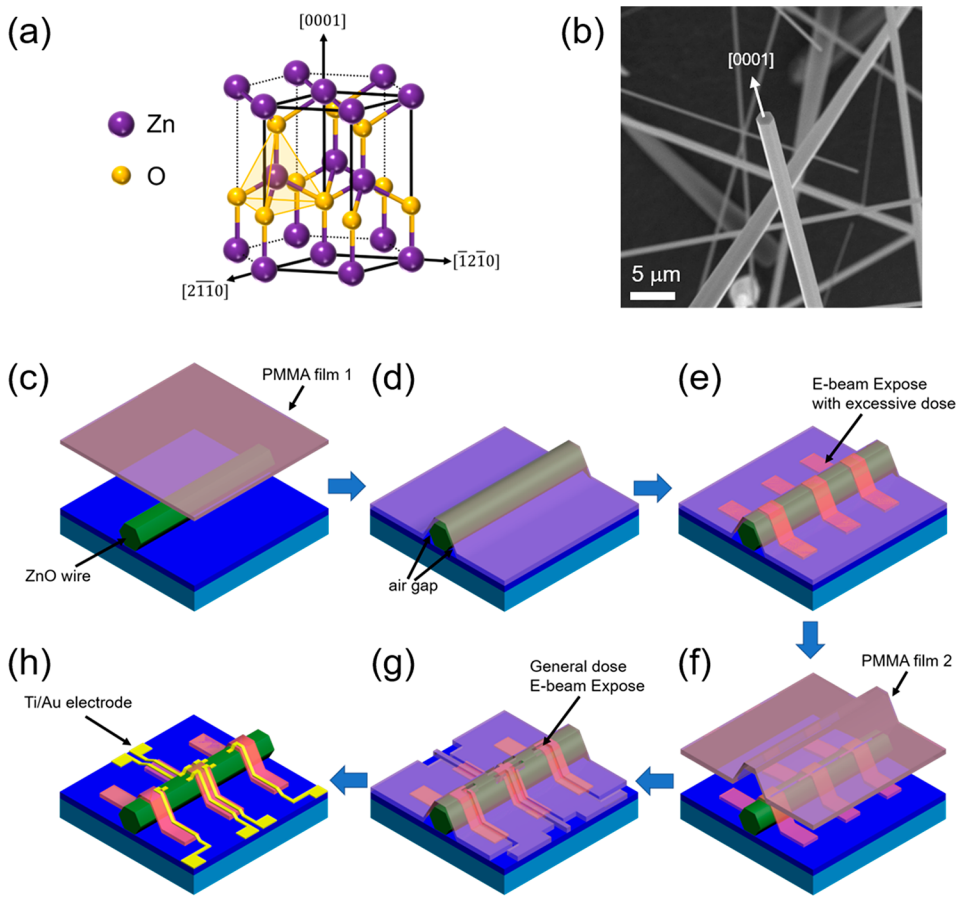

Figure 1. Image of ZnO microwires and schematics of the device fabrication process. (a) Schematic of the ZnO crystal structure. (b) SEM image of ZnO microwires grown on the Si (001) substrate. (c) A PMMA film was transferred onto the ZnO microwire. (d) Transferred PMMA covered the ZnO with an air gap at the side of the ZnO microwire. (e) Cross-linked PMMA structures were defined by excessive electron beam exposure. (f) The second PMMA film was transferred on the ZnO microwire with a suspended PMMA ribbon structure. (g) Nanoscale electrode patterns were defined by the electron beam lithography process. (h) The fabrication of the device structure was completed after metal deposition, followed by a liftoff process.

ing chemical vapor deposition (CVD), molecular beam epitaxy (MBE), and sol–gel processes.[13−15] Of these methods, CVD and MBE are used to produce high-quality materials by maintaining the temperature, pressure, and flow rate of elements during growth processes. Nevertheless, it remains difficult to prepare a material with a perfectly uniform size and consistent material performance from each nano-/microwire. Our previous report found that the composition of semiconducting nanowires might vary along the axial direction, even though the nanowire growth parameters were constantly controlled during MBE growth.[16] In this case, the electrical properties of the nanowire might also differ according to the local position of the nanowire. Therefore, it is important to directly investigate the electrical properties of nano-/microwires at specified positions by defining electrode structures on the desired spatial area.

In this study, we investigated the electrical properties of a single facet of an individual ZnO microwire structure. Hall bar-type electrodes were electrically connected only between the bottom circuit and top facet of the ZnO microwire, while suspended electron-beam-resist ribbon structures were fabricated to passivate the other areas. The carrier density and mobility at the local area along the axial direction of the ZnO microwire were estimated by measuring the current–voltage (I–V) and Hall characteristics under various magnetic fields. The geometry of the electrodes defined by our technique made it possible to reveal that the doping concentration could be sensitively changed during synthesis of the ZnO microwire.

2. RESULTS AND DISCUSSION

Well-crystallized ZnO microwires were synthesized by the CVD method, as shown in Figure 1b. The crystal structure and material characterization of the ZnO microwire were studied in our previous report.[17] A suspended and cross-linked poly(methyl methacrylate) (PMMA) ribbon structure was created to make the electrical connections between the bottom substrate and the top facet of the ZnO microwire. Figure 1 shows schematics of the fabrication procedure of the electrodes for Hall measurements on the ZnO microwire. Spin-coated PMMA was prepared from the original substrate and transferred to a ZnO microwire (Figure 1c). An air gap between the transferred PMMA and ZnO microwire appeared after the transfer process, as shown in Figure 1d, owing to the height differences. Then, an excessive dose of the electron beam was irradiated to establish the cross-linked and suspended PMMA ribbon, bridging the bottom substrate and the top of the ZnO microwire (Figure 1e). The detailed fabrication conditions and procedures for fabricating the PMMA bridges are described in our previous report.[10] Another piece of PMMA film was transferred onto the ZnO and cross-

https://doi.org/10.1021/acsaelm.2c00179
ACS Appl. Electron. Mater. 2022, 4, 2346−2352

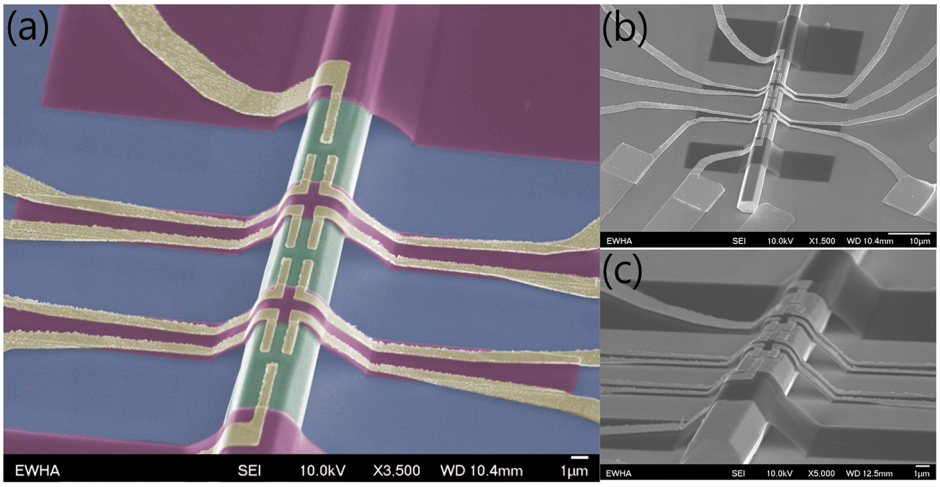

Figure 2. Scanning electron microscopy (SEM) images of the ZnO microwire device. (a) False color SEM image of the device. Electrodes (yellow) were developed on the top facet of the ZnO microwire (green) through suspended and cross-linked PMMA (dark purple). SEM images showing (b) the device with a microscale outer circuit and (c) a tilted view of the device.

linked PMMA bridge (Figure 1f), and the electrode pattern was defined with a normal dose of electron beam irradiation (Figure 1g). Fabrication of the electrodes for Hall measurement was completed after the metal deposition and liftoff processes (Figure 1h).

Figure 2 displays scanning electron microscopy (SEM) images of the device structure for analysis of the Hall effect on the top surface of a ZnO microwire. Ten electrodes were placed on top of the ZnO microwire. The electrodes were integrated with ZnO from the bottom circuit to the top facet of the ZnO microwire via cross-linked PMMA structures (Figure 2b). The tilted SEM image in Figure 2c clearly shows that the cross-linked PMMA stably bridges the bottom substrate and the top of the ZnO microwire, with a height difference of approximately 3.5 μm. The cross-linked PMMA was also used as a passivation layer so the metal electrodes could only probe the top facet of the ZnO microwire surfaces.

The electrical transport properties of the fabricated ZnO microwire devices were measured. Figure 3a,b shows optical microscopy (OM) images of a ZnO microwire device, providing an overview of the device connected to the outer electrical circuit and an enlarged image of the top facet of the ZnO microwire, respectively. It was noticed that the ZnO microwire is slightly tapered from source to drain electrodes, which corresponds from the top to the bottom of the microwire in the growth condition. The cross-sectional area decreased by about 0.09 μm^2 per 1 μm along the longitudinal direction, which could be estimated from the SEM image, as shown in Figure S1 in the Supporting Information. Figure 3c presents a schematic of the electrode geometry and measurement configuration for investigating the transport properties.

The electrical transport properties were measured using a Keithley semiconductor characterization system (SCS4200) with a vacuum probe station. Figure 4a,b displays the measurement results of the length-dependent resistances in the axial direction (R_{xx}) on the top facet of the ZnO microwire. The resistance R_{xx1} (R_{xx2}) values were estimated from the 2-probe $I-V$ characteristics (Figure S2) between the drain (source) and upper (lower) part of the side electrodes, as shown in Figure 3c.

Figure 4a,b shows plots of the resistances, R_{xx1} and R_{xx2}, versus the distances between the drain and upper-side

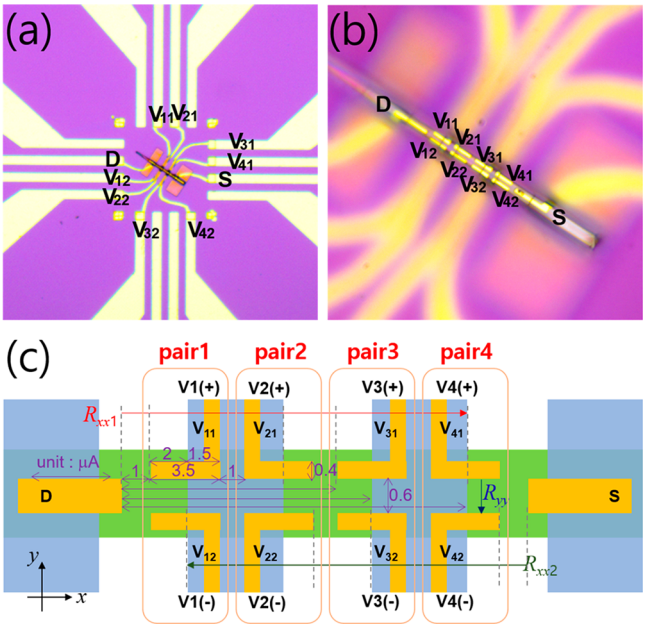

Figure 3. (a) Optical microscopy (OM) image of a ZnO microwire device with the configuration of circuit connections. (b) OM image focused on the top of the ZnO microwire. (c) Schematic of the electrode configuration on the top facet of the ZnO microwire, with scales.

electrodes, and source and lower-side electrodes, respectively. The resistance values were found to increase linearly as the channel length increased. Contact resistance values of 11.17 and 6.52 kΩ were estimated using the transfer length method from Figure 4a,b, respectively. Meanwhile, Figure 4c displays the resistance values measured from the four pairs of side electrodes facing each other. The 2-probe resistance values were determined to be in the range 3.80−4.85 kΩ, indicating that the contact resistances on the side electrodes are relatively less than those on the source/drain electrode. It is considered that the differences in the contact resistances for drain (source) and upper (lower) electrodes are caused by the geometry of the electrode structures. An unexpected poor contact interface

https://doi.org/10.1021/acsaelm.2c00179
ACS Appl. Electron. Mater. 2022, 4, 2346−2352

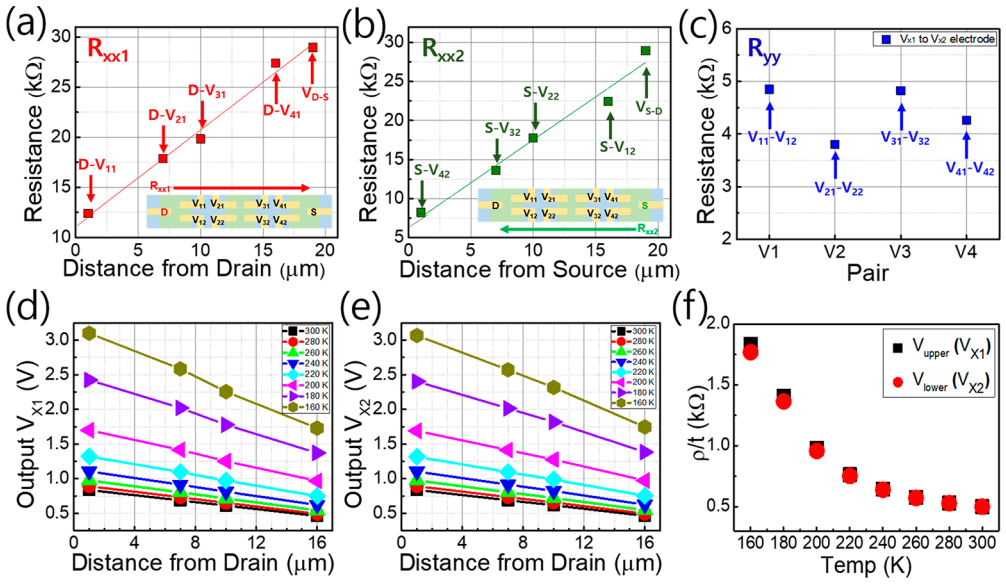

Figure 4. Length-dependent resistances (R_{xx1} and R_{xx2}) of the ZnO microwire measured between (a) drain and upper-side electrodes, and (b) source and lower-side electrodes. (R_{SD} indicates the resistance measured between the source and drain electrodes.) (c) Resistance values (R_{yy}) measured between the pairs of side electrodes in the vertical direction. Measurement results of output voltage from the drain electrode to (d) upper- and (e) lower-side electrodes, plotted with respect to the distance between each side and drain electrode. (f) Temperature dependence of resistivity estimated from the slopes in parts d and e.

created during the metal deposition process could significantly affect source and drain electrodes more than the side ones.

Nevertheless, the contact resistance presented in this paper was found to be over 100 times smaller than that previously reported on a ZnO microwire device fabricated using the same method[10] with cross-linked PMMA bridge structures. We have improved our device fabrication technique by using the dry transfer method to deposit the ZnO wire on the substrate and oxygen plasma treatment just before metal evaporation. Owing to the solid and dependable electrical contact between the electrodes and the ZnO microwire, the Hall effect could be investigated at a specific region on the ZnO surface in a reliable manner, as described in the next section.

Figure 4d,e shows the measurement results of the output voltage plotted against the distance from the drain electrode to each upper-side (lower-side) electrode at various temperatures in the range 160−300 K. The current bias of 20 μA was applied between the source and drain electrodes to obtain the output voltages. The slopes of the measurement points at a given temperature, as displayed in Figure 4d,e, can be estimated from the resistances at each segment of the ZnO microwire. All of the distance-dependent output voltages exhibit linear curves with no significant slope changes at each segment. Thus, the resistivity values at each area do not exhibit noticeable differences along the axis of the ZnO microwire. Figure 4f presents the temperature dependence of the resistivity values estimated from the slopes in Figure 4d,e. Typical semiconducting behavior is apparent, as expected from ZnO. The resistivity values obtained through the upper- and lower-side electrodes are almost the same, particularly in the high-temperature region. Because the contact resistance value at the upper electrodes is higher than that at the lower electrodes, as shown in Figure 4a,b, the energy barrier differences related to the contact resistance are considered to cause the slight differences in the resistivity values in the low-temperature region.

The Hall effect on the top facet of the ZnO microwire was measured using a physical property measurement system (Quantum Design PPMS) by reducing the temperature from 300 to 160 K and sweeping the magnetic field up to ±9 T. A constant electric current of 20 μA was applied along the top facet of the ZnO microwire through the source and drain electrodes. The Hall voltage values were measured from the four side electrode pairs, while magnetic field sweeping was performed (0 T → 9 T → −9 T → 0 T) via 0.1 T steps in the direction perpendicular to the top facet of the ZnO microwire. The measured Hall voltages linearly increased as the magnetic field increased.

Figure 5a shows the results of the Hall resistances measured for each pair of side electrodes at various temperatures. It is apparent that the resistances, which were measured from all pairs, increased exponentially with decreasing temperature. This transport behavior in the temperature range 160−300 K is considered to be governed by thermionic emission.[18] Figure 5b shows the corresponding carrier concentrations estimated from the measured Hall resistance values.[18,19] The charge carrier concentration on the surface of our ZnO microwire varied from 1×10^{13} to 7×10^{13} cm^{-2} as the temperature increased from 160 to 300 K. The carrier concentrations determined in our work are of a similar order of magnitude to those reported in previous studies using different methods, such as measuring the transconductance of ZnO nanowire-based field-effect transistors (FETs)[20] and scanning probe microscopy measurements with ZnO film structures.[21] Figure 5c displays the Hall mobility values estimated from the Hall resistances in Figure 5a and the axial-direction resistivity values in Figure 4f at various temperatures.

The insets in Figure 5a−c show the Hall resistance, carrier concentration, and Hall mobility values at room temperature according to the distance of the side electrode pairs from the drain electrode, respectively. Interestingly, the Hall resistance and Hall mobility values increase as the distance between the side electrode pairs and drain electrodes, which is indicated in

https://doi.org/10.1021/acsaelm.2c00179
ACS Appl. Electron. Mater. 2022, 4, 2346−2352

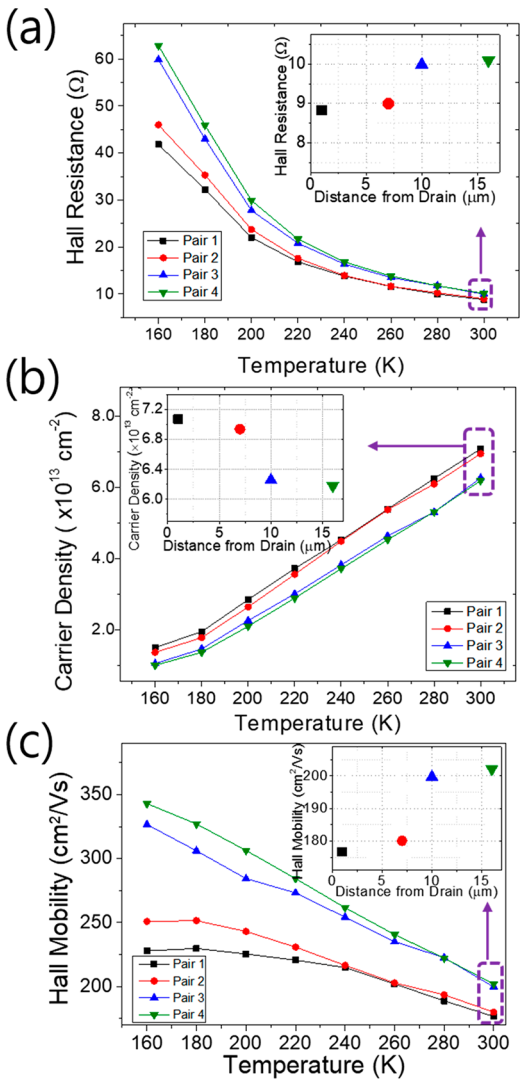

Figure 5. (a) Hall resistances measured from each pair of side electrodes at various temperatures. (b) Corresponding charge carrier concentrations estimated from Hall resistance values. (c) Hall mobilities estimated from Hall resistance and resistivity values at various temperatures. Insets in panels a–c show the Hall resistance, carrier concentration, and Hall mobility values, repectively, at room temperature according to the distance of the side electrode pairs from the drain electrode, as indicated in Figure 3c.

Figure 3c, increases. Accordingly, the corresponding carrier concentration decreases as the distance from the drain to the side electrodes increases. We think that the difference of carrier concentration along the axis of the ZnO microwire was attributed to a variation of synthesis atmosphere during microwire production. While the ZnO microwire is vertically grown, the oxygen flow rate could be slightly different along the height of the chamber so that the oxygen vacancy at the surface of ZnO might vary from the bottom to the top of microwire. This influence also appears in the SEM and OM images, presented in Figures 2 and 3, respectively, showing that the overall thickness along the ZnO microwire slightly tapers from the source to the drain electrode (i.e., from the position of electrode pair 4 to pair 1 indicated in Figure 3c). Through microscopic observation after the synthesis of our ZnO microwire,[17] it was found that tapering occurred from the top to the bottom of the wire. Based on the results mentioned above, it can be considered that the carrier density is higher at the bottom position of the microwire and then decreases as the wire grows. As discussed in the previous section, no noticeable resistivity differences were observed at each segment of the side electrodes without application of a magnetic field. Because the length and cross-sectional area are included when the resistance is measured, these geometrical parameters might make it difficult to differentiate the resistivity, especially with a small variation, and, consequently, smear the position dependence of the intrinsic electrical resistivity information. However, the Hall measurement enables us to obtain the carrier concentration without being affected by the dimensionality factors of the materials. This is considered to be the reason why the variation in carrier density was observed via Hall measurement but not from the resistivity measurement. Moreover, energy-dispersive X-ray spectroscopy (EDS) along with a ZnO microwire axis also showed that the oxygen ratio in the microwire surface increases as the measurement point moves from the thin to thick position of the wire (see Figure S2 in the Supporting Information). This result implies that the oxygen vacancy can cause charge carrier density variation on the surface of the ZnO microwire, which is consistent with our Hall measurement results.

Using our unique device structure comprising a cross-linked PMMA bridge, electrical contacts could be created with only one facet of the microwire such that the electrical properties could be directly probed at a specific area on the surface of the ZnO microwire. In particular, variation in the carrier concentration at different positions on the ZnO microwire surface could be accurately investigated from the Hall measurements through the four pairs of side electrodes. Several studies have determined the charge carrier concentration of ZnO micro-/nanostructures by realizing FET devices.[22−24] In those previous works, the carrier concentrations were estimated by obtaining the subthreshold swing values from transfer curve measurements of FETs. In this case, only the average carrier concentration distributed along the FET channel is known. Furthermore, it is not easy to determine the gate capacitance value, which is a crucial parameter for obtaining carrier concentration through the transfer characteristics of an FET. Thus, it is generally considered that the estimation of the carrier concentration from FET characteristics is relatively less accurate than that obtained from direct Hall measurements. Meanwhile, an advantage of the device presented herein is that the carrier concentration can be determined at a specific point on the ZnO surface in a direct and reliable manner.

From the experimental results of our devices, it was found that changes in the carrier concentration, particularly on the surface of the microwire, were sensitive to the position of the wire. Huh et al.[16] reported a similar phenomenon, demonstrating a self-induced compositional variation at the top and root of a GaAsSb nanowire. In their case, the synthesis parameters of the nanowire growth were also maintained constant using an MBE method, which is generally known to control the parameters in a highly consistent manner. Moreover, our previous work implied that the synthesis environments at the bottom and top positions of the micro-/nanowire might not be perfectly consistent, although the parameters of CVD were kept constant while growing the ZnO microwires. As a result, the carrier concentration can vary at different wire positions.

https://doi.org/10.1021/acsaelm.2c00179
ACS Appl. Electron. Mater. 2022, 4, 2346−2352

3. CONCLUSIONS

In this study, electrical transport measurements were performed on a single facet of an individual ZnO microwire. A cross-linked PMMA ribbon structure functioned as a bridge between the substrate and the ZnO microwire such that an electrical connection between the bottom circuit and top facet of the microwire could be defined. By overlapping the electrode patterns on the suspended PMMA bridge structures through careful electron beam alignment, only the top facet of the ZnO microwire was in contact with the electrodes, while the other parts were passivated. Two source/drain electrodes and four pairs of side electrodes were fabricated on the top surface of the ZnO microwire, which was approximately 3.5 μm above the bottom substrate.

The $I-V$ measurements with various electrode pairs demonstrated that stable electrical contacts formed on the ZnO surface with contact resistance values of less than 11.2 kΩ. These values are sufficiently low for investigating the Hall properties on the surface of the ZnO microwire. Hence, the Hall effect was investigated at various temperatures, and the results were used to estimate the charge carrier concentration and mobility values. The carrier concentration values on the ZnO surface gradually decreased from the bottom to the top position of the microwire. This indicates that the carrier concentration, particularly on the surface of the micro-/nanowire, was sensitive to the synthesis environment, even though the growth parameters were controlled. Our unique device fabrication method can be applied to define nanoscale electrical probes on microscale structures in a stable and reliable manner.

4. EXPERIMENTAL SECTION

Device Fabrication. ZnO microwires were synthesized via CVD on a Si (001) substrate. A ZnO and graphite powder mixture (ZnO:C = 1:1) was used as the initial material for ZnO microwire production. The synthesis parameters, i.e., growth temperature and gas flow rate, were precisely controlled during the CVD process. From the X-ray diffraction and photoluminescence spectra, it was found that the synthesized microwires were well-crystallized with few defects. Details of the microwire production procedure and material characterization are described in our previous report.[17] The thicknesses of the synthesized ZnO microwires were approximately 3 ± 0.5 μm.

■ ASSOCIATED CONTENT

Supporting Information

The Supporting Information is available free of charge at https://pubs.acs.org/doi/10.1021/acsaelm.2c00179.

Detailed dimensions of the ZnO microwire; energy-dispersive X-ray spectroscopy along the axis; $I-V$ characteristics; and charge density variation in various devices along the axial direction (PDF)

■ AUTHOR INFORMATION

Corresponding Authors

Haeyong Kang − *Department of Physics, Pusan National University, Busan 46241, Korea;* orcid.org/0000-0002-8799-3935; Email: haeyong.kang@pusan.ac.kr

Sang Wook Lee − *Department of Physics, Ewha Womans University, Seoul 03760, Korea;* orcid.org/0000-0003-2265-4761; Email: leesw@ewha.ac.kr

Authors

Yoojoo Yun − *Department of Physics, Pusan National University, Busan 46241, Korea*

Dong Hoon Shin − *Kavli Institute of Nanoscience, Delft University of Technology, 2628 CJ Delft, The Netherlands*

Hakseong Kim − *Korea Research Institute of Standards and Science (KRISS), Daejeon 34113, Korea*

Jun Hee Choi − *Defense Agency for Technology and Quality, Jinju, Gyeongsangnam-do 52851, Korea*

Hyunjeong Jeong − *Department of Physics, Ewha Womans University, Seoul 03760, Korea*

Dongseok Suh − *Department of Energy Science, Sungkyunkwan University, Suwon 16419, Korea;* orcid.org/0000-0002-0392-3391

Complete contact information is available at: https://pubs.acs.org/10.1021/acsaelm.2c00179

Author Contributions

$^{\nabla}$Y. Yun, D. H. Shin, and H. Kim contributed equally to this work.

Notes

The authors declare no competing financial interest.

■ ACKNOWLEDGMENTS

This work was supported by the Basic Science Research Program (NRF-2022R1A2B5B01001640, NRF-2022R1A4A2000835, NRF-2021R1A6A1A10039823, and NRF- 2021R1A2C2013289), Global Research and Development Center Program (2018K1A4A3A01064272) through the National Research Foundation of Korea (NRF) funded by the Ministry of Education, and by Basic Science Institute (National research Facilities and Equipment Center) grant funded by the Ministry of Education (2021R1A6C101A429). This work was also supported by the Technology Innovation Program (20006492) funded by the Ministry of Trade, Industry & Energy.

■ REFERENCES

(1) Kolodziejczak-Radzimska, A.; Jesionowski, T. Zinc Oxide-From Synthesis to Application: A Review. *Materials* **2014**, *7*, 2833−2881.

(2) Zhang, Y. Y.; Ram, M. K.; Stefanakos, E. K.; Goswami, D. Y. Synthesis, Characterization, and Applications of ZnO Nanowires. *J. Nanomater.* **2012**, *2012* (20), 624520.

(3) Arnold, M. S.; Avouris, P.; Pan, Z. W.; Wang, Z. L. Field-Effect Transistors Based on Single Semiconducting Oxide Nanobelts. *J. Phys. Chem. B* **2003**, *107*, 659−663.

(4) Yi, G. C.; Wang, C. R.; Park, W. I. ZnO Nanorods: Synthesis, Characterization and Applications. *Semicond. Sci. Technol.* **2005**, *20*, S22−S34.

(5) Su, M. M.; Zhang, T. L.; Su, J.; Wang, Z.; Hu, Y. M.; Gao, Y. H.; Gu, H. S.; Zhang, X. H. Homogeneous ZnO Nanowire Arrays P-N Junction for Blue Light-Emitting Diode Applications. *Opt. Express* **2019**, *27*, A1207−A1215.

(6) Vanmaekelbergh, D.; van Vugt, L. K. ZnO Nanowire Lasers. *Nanoscale* **2011**, *3*, 2783−2800.

(7) Bae, M. Y.; Min, K. W.; Yoon, J.; Kim, G. T.; Ha, J. S. Electronic Properties of Light-Emitting P-N Hetero-junction Array Consisting of p(+)-Si and Aligned n-ZnO Nanowires. *J. Appl. Phys.* **2013**, *113*, 084310.

(8) Hu, L.; Liao, Q.; Xu, Z.; Yuan, J.; Ke, Y.; Zhang, Y.; Zhang, W.; Wang, G. P.; Ruan, S.; Zeng, Y.; Han, S. Defect Reconstruction Triggered Full-Color Photodetection in Single Nanowire Phototransistor. *ACS Photonics* **2019**, *6*, 886−894.

(9) Li, F.; Meng, Y.; Kang, X.; Yip, S.; Bu, X.; Zhang, H.; Ho, J. C. High-Mobility In and Ga co-doped ZnO Nanowires for High-

Performance Transistors and Ultraviolet Photodetectors. *Nanoscale* **2020**, *12*, 16153−16161.
(10) Kim, H.; Yun, H.; Yoon, H. A.; Lee, S. W. Integrating ZnO Microwires with Nanoscale Electrodes Using a Suspended PMMA Ribbon for Studying Reliable Electrical and Electromechanical Properties. *Adv. Energy Mater.* **2014**, *4*, 1301973.
(11) Wang, X. D.; Zhou, J.; Song, J. H.; Liu, J.; Xu, N. S.; Wang, Z. L. Piezoelectric Field Effect Transistor and Nanoforce Sensor Based on a Single ZnO Nanowire. *Nano Lett.* **2006**, *6*, 2768−2772.
(12) Wang, Z. L.; Song, J. H. Piezoelectric Nanogenerators Based on Zinc Oxide Nanowire Arrays. *Science* **2006**, *312*, 242−246.
(13) Zhao, X. X.; Nagashima, K.; Zhang, G. Z.; Hosomi, T.; Yoshida, H.; Akihiro, Y.; Kanai, M.; Mizukami, W.; Zhu, Z. T.; Takahashi, T.; Suzuki, M.; Samransuksamer, B.; Meng, G.; Yasui, T.; Aoki, Y.; Baba, Y.; Yanagida, T. Synthesis of Monodispersedly Sized ZnO Nanowires from Randomly Sized Seeds. *Nano Lett.* **2020**, *20*, 599−605.
(14) Kennedy, O. W.; Coke, M. L.; White, E. R.; Shaffer, M. S. P.; Warburton, P. A. MBE Growth and Morphology Control of ZnO Nanobelts with Polar Axis Perpendicular to Growth Direction. *Mater. Lett.* **2018**, *212*, 51−53.
(15) Chang, P. C.; Fan, Z. Y.; Wang, D. W.; Tseng, W. Y.; Chiou, W. A.; Hong, J.; Lu, J. G. ZnO Nanowires Synthesized by Vapor Trapping CVD Method. *Chem. Mater.* **2004**, *16*, 5133−5137.
(16) Huh, J.; Yun, H.; Kim, D. C.; Munshi, A. M.; Dheeraj, D. L.; Kauko, H.; van Helvoort, A. T. J.; Lee, S.; Fimland, B. O.; Weman, H. Rectifying Single GaAsSb Nanowire Devices Based on Self-Induced Compositional Gradients. *Nano Lett.* **2015**, *15*, 3709−3715.
(17) Kim, H.; Jung, U. S.; Kim, S. I.; Yoon, D.; Cheong, H.; Lee, C. W.; Lee, S. W. Young's Modulus of ZnO Microwires Determined by Various Mechanical Measurement Methods. *Curr. Appl. Phys.* **2014**, *14*, 166−170.
(18) Sze, S. M. *Semiconductor Devices, Physics and Technology*; Wiley: New York, 2002.
(19) Ashcroft, N. W.; Mermin, N. D. *Solid State Physics*; Holt: New York, 1976.
(20) Oh, H.; Kim, J. J.; Lee, J. O.; Kim, S. S. Temperature Dependent Intrinsic Carrier Mobility and Carrier Concentration in Individual ZnO Nanowire with Metal Contacts. *J. Korean Phys. Soc.* **2011**, *58*, 291−296.
(21) Maragliano, C.; Lilliu, S.; Dahlem, M. S.; Chiesa, M.; Souier, T.; Stefancich, M. Quantifying Charge Carrier Concentration in ZnO Thin Films by Scanning Kelvin Probe Microscopy. *Sci. Rep.* **2015**, *4*, 4203.
(22) Choe, M.; Park, W.; Kang, J. W.; Jeong, S.; Hong, W. K.; Lee, B. H.; Park, S. J.; Lee, T. Investigation of Threshold Voltage Instability Induced by Gate Bias Stress in ZnO Nanowire Field Effect Transistors. *Nanotechnology* **2012**, *23*, 485201.
(23) Song, S.; Hong, W. K.; Kwon, S. S.; Lee, T. Passivation Effects on ZnO Nanowire Field Effect Transistors under Oxygen, Ambient, and Vacuum Environments. *Appl. Phys. Lett.* **2008**, *92*, 263109.
(24) Kim, D. S.; Richters, J. P.; Scholz, R.; Voss, T.; Zacharias, M. Modulation of Carrier Density in ZnO Nanowires without Impurity Doping. *Appl. Phys. Lett.* **2010**, *96*, 123110.

https://doi.org/10.1021/acsaelm.2c00179
ACS Appl. Electron. Mater. 2022, 4, 2346−2352